Robotica (2018) volume 36, pp. 448–462. © Cambridge University Press 2017
doi:10.1017/S0263574717000492

Design and implementation of a variable stiffness actuator based on flexible gear rack mechanism

Wei Wang*†, Xiaoyue Fu†, Yangmin Li‡ and Chao Yun†

† *School of Mechanical Engineering and Automation, Beihang University, Beijing, P.R. China. E-mails: 1582790103@qq.com, cyun18@vip.sina.com*
‡ *Department of Industrial and Systems Engineering, the Hongkong Polytechnic University, Hongkong S.A.R. E-mail: yangmin.li@polyu.edu.hk*

(Accepted September 17, 2017. First published online: November 10, 2017)

SUMMARY
Variable stiffness can improve the capability of human–robot interacting. Based on the mechanism of a flexible rack and gear, a rotational joint actuator named vsaFGR is proposed to regulate the joint stiffness. The flexible gear rack can be regarded as a combination of a non-linear elastic element and a linear adjusting mechanism, providing benefits of compactness. The joint stiffness is in the range of 217–3527 N.m/rad, and it is inversely proportional to the 4th-order of the gear displacement, and nearly independent from the joint angular deflection, providing benefits of quick stiffness regulation in a short displacement of 20 mm. The gear displacement with respect to the flexible gear rack is perpendicular to the joint loading force, so the power required for stiffness regulating is as low as 14.4 W, providing benefits of energy saving. The working principles of vsaFGR are elaborated, followed by presentation on the mechanics model and the prototype. The high compactness, great stiffness range and low power cost of vsaFGR are proved by simulations and experiments.

KEYWORDS: Variable stiffness, Flexible gear rack, Stiffness regulation, Robot, Joint actuator

1. Introduction

Future robots are expected to be intrinsically safe and highly energy efficient. Variable Stiffness Actuators (VSA) have played a very important role in improving the robot's adaptability in the fields of human–robot interaction and energy saving.[1–5] Robotic applications requiring variable stiffness can be divided into three groups in terms of improving robot–human interaction, adjusting natural dynamics and saving energy for mobile platforms.[3,4] It is reported that VSAs offer the possibility to move the load more quickly and safely than other solutions based on ideally rigid or passively flexible joints.[1]

Years ago, Remote Center Compliance (RCC)[6] was designed for robotic assembling applications to provide a certain degree of passive compliance when contact happened. Then passive compliant actuators are widely used in robot joints, such as the well-known Series Elastic Actuator (SEA).[7,8] The joint compliance is decided by the characteristics of spring, while the apparent compliance cannot be adjusted during operation. Some special material such as piezoelectric substance,[9] MR fluid,[10] silicone-rubber cushions,[11] thermo-mechanical material,[12] arc-shaped magnets[13] and nylon coiled fibers[14] are also employed in the joint compliant actuator for different applications.

To imitate the mechanism of biceps and triceps in the human arm, an antagonistic type known as bio-inspired VSA,[15] has been designed. Many prototypes of antagonistic VSA have been developed for different robotic applications in the last decade, such as VSA,[16,17] Actuators with Mechanically Adjustable Series Compliance (AMASC),[18] Pneumatic Artificial Muscles (PAM),[19] Quasi-Antagonistic Joints (QA-Joint)[20] and Cable Based Active Variable Stiffness Module.[21]

* Corresponding author. E-mail: jwwx@163.com

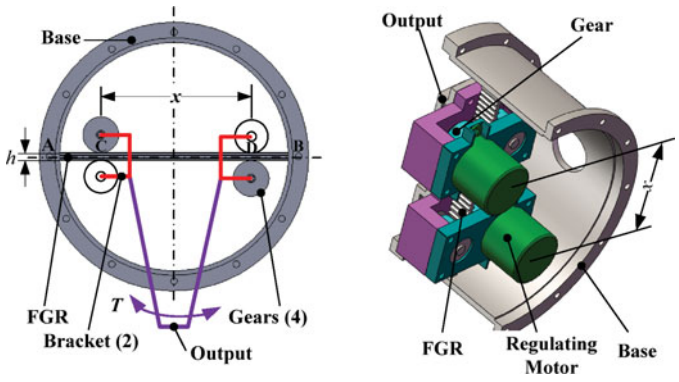

Fig. 1. Working principles of vsaFGR.

It is worth noting that variable-stiffness joint actuators with active regulating mechanisms have been extensively explored in recent years. Among them, many research efforts have been made on the variable stiffness issue based on the lever mechanism through changing the effective arm length via varying the spring locations,[22–24] changing the point where the force is applied[25] and changing the lever ratio by moving the location of pivot position.[26–28] This type of VSA combines a linear spring with the adjusting mechanism working in a nonlinear way. The Jack Spring,[29] Mechanically Adjustable Compliance and Controllable Equilibrium Position Actuator (MACCEPA),[30] VS Joint,[31] Safe Joint Mechanism[32] and Cam Disc Variable Stiffness Mechanisms (VSM)[33] can be regarded as this type. Among this type of VSA, the nonlinear adjusting mechanism has negative effects on the compactness.

Besides linear springs, the nonlinear elastic element, such as the leaf spring and the buckled strip,[34] can be combined with the linear adjusting mechanism. The leaf spring and the ball screw mechanism are exploited in the Mechanical Impedance Adjuster (MIA).[35] The Variable Negative Stiffness Actuation (VNSA) achieves variable stiffness actuation based on the nonlinear deflection characteristics of buckling beams.[36] For the Variable Stiffness Joints (VSJ)[37] and VSM,[38] when the rollers slide on the flat leaf spring in a linear way, the bending stiffness of the spring is changed in a nonlinear way. Among all VSAs, the power cost and the dimension requirement on the regulating process could be further reduced.

Based on our previous work of vsaMGR,[39] this paper aims to vary joint stiffness by employing a more efficient regulating mechanism at the cost of less energy. The second purpose is to design and test a high-order profile of stiffness regulation, and achieve a larger range of stiffness in a short regulating displacement.

As a result of the flexible gear rack (FGR), a new type of VSA is proposed. Compared with the existing VSA, the major novelty of vsaFGR lies in that the nonlinear elastic element and the linear adjusting mechanism are combined into one element. FGR is considered as a combination of a leaf spring and gear teeth, as shown in Fig. 1. The gear teeth are used to change the force-acting position in a linear way, and the leaf spring is acting as the nonlinear elastic element. Then, the mechanical structure could occupy a relatively small volume. Second, the stiffness range is decided by the bending stiffness of the leaf spring and the (-4)-order of the displacement of the gears engaged with FGR. It provides a fast response to achieve an expected joint stiffness (from 217 to 3527 N.m/rad) in a short stroke (20 mm). Finally, because the adjusting force is on the tangential direction of the adjusting gears, and the loading force is acting towards the radial direction, very small amount of power (14.4 W) is required during the stiffness regulation process. This provides more adaptability for power hard-to-get applications. The overall volume and the regulating power of our prototype are smaller than those of VSJ[36] by 27% and 92%, respectively. Based on these ideas, a prototype and its stiffness range are designed. It will be used as an ankle joint of a future walking robot.

This paper is organized as follows. In Section 2, the working principle of vsaFGR is explained. The mechanics model is presented in Section 3. The fabrication of vsaFGR prototype is discussed in Section 4. The performance of vsaFGR prototype in regulating the stiffness is simulated in Section 5. Experimental studies are conducted in Section 6. Finally, the conclusion and future works are given in the last section.

https://doi.org/10.1017/S0263574717000492 Published online by Cambridge University Press

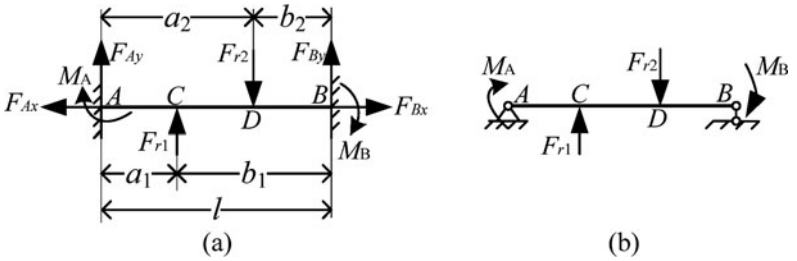

Fig. 2. Mechanics model of flexible gear rack. (a) A complete model. (b) An equivalent model.

2. Working Principles of vsaFGR

A specific type of rack and gear mechanism, FGR combines the gear teeth and the flexible beam into one element. The height of FGR h is fairly small, typically in the range of from 1 mm to 2 mm. It is fixed at two ends, a two-end fixture which is considered as a flexible Bernoulli beam with two clamped constraints. It provides great slope when exerted by a radial load. Involute teeth are cut on both sides of FGR, and two pairs of spur gears are installed to mesh with FGR as shown in Fig. 1. The external force couple T is exerted in the radial direction of FGR via gear engagements. Each pair of gears are driven by a regulating motor in a synchronous way, and the gears translate along FGR while engaged. The variable meshing points are regarded as the varying acting points of the radial load F. The displacement between the gears x is controlled in order to regulate the angular stiffness of the rotational robot joint.

In Fig. 1, an external torque $T = Fx$, is applied on the link in an anticlockwise/clockwise direction. The joint stiffness is dependent on x. If x is decreased, the slope of FGR θ is increased. The angular displacement of the link δ is increased, and the apparent stiffness of the joint K is decreased in the anticlockwise/clockwise direction. If $x = 0$, θ becomes infinite, and K becomes zero. On the other side, if x is increased, K is increased in the anticlockwise/clockwise direction. If x is right equal to the diameter of the base, θ becomes zero, and the joint becomes full rigid. With this new type of regulating mechanism, K is varied in both directions by controlling x.

The benefits of FGR regulating mechanism can be summarized in two aspects. First of all, x is tangential to the pitch circle of gears and F is along the radial direction of the pitch circle. They are perpendicular to each other, and the active torque required to x could be very small. Consequently, the regulating gears can be driven with very small motors. Second, the elastic element and the stiffness regulating mechanism have been combined into FGR, and a compact joint actuator can be obtained. In our prototype shown in Section 4, the regulating power is 14.4 Watt, and its overall dimension is $\Phi 118 \times 160$ mm^3, providing great benefits for walking robots or mobile platforms.

3. Mechanics Model of vsaFGR

As FGR is fixed at both ends, it can be modeled as a static indeterminate beam as shown in Fig. 2(a). The model of joint stiffness K can be established by the following steps.

The deformation is assumed to be linear and small enough, and the horizontal force components at both ends F_{Ax} and F_{Bx} are ignored, which leads to

$$F_{Ax} = 0, \quad F_{Bx} = 0 \tag{1}$$

The redundant constrains of the static indeterminate beam are removed, and it is converted into an equivalent system, as shown in Fig. 2(b). Because of the deformation compatibility condition, the slopes θ_A and θ_B at the ends of A and B are assumed to be zero. Then, we have

$$\theta_A = 0, \quad \theta_B = 0 \tag{2}$$

Using the method of linear superposition, we have the two slopes contributed by the radial force components F_{r1}, F_{r2} and the supporting moment components M_A, M_B

https://doi.org/10.1017/S0263574717000492 Published online by Cambridge University Press

$$\theta_A = -\frac{F_{r2}a_2b_2(l+b_2)}{6EIl} - \frac{F_{r1}a_1b_1(l+b_1)}{6EIl} - \frac{M_Al}{3EI} + \frac{M_Bl}{6EI} \tag{3}$$

$$\theta_B = -\frac{F_{r2}a_2b_2(l+b_2)}{6EIl} - \frac{F_{r1}a_1b_1(l+a_1)}{6EIl} - \frac{M_Al}{6EI} + \frac{M_Bl}{6EI} \tag{4}$$

where E and I are the modulus of elasticity of material and the moment of inertia of beam section, respectively. Substituting (3) and (4) into (2), we have

$$M_A = \frac{-F_{r2}b_2^2\,(l-b_2) - F_{r1}a_1(l-a_1)^2}{l^2} \tag{5}$$

$$M_B = \frac{F_{r2}b_2(l-b_2)^2 + F_{r1}a_1^2\,(l-a_1)}{l^2} \tag{6}$$

Using the method of linear superposition, we have the nominal deflection at the engaging points C and D.

$$\omega_{r1} = \omega_{P_1 1} + \omega_{P_2 1} + \omega_{M_{A1}} + \omega_{M_{B1}} \tag{7}$$

$$\omega_{r2} = \omega_{P_1 2} + \omega_{P_2 2} + \omega_{M_{A2}} + \omega_{M_{B2}} \tag{8}$$

ω_{r1}, $\omega_{P_1 1}$, $\omega_{P_2 1}$, $\omega_{M_{A1}}$, $\omega_{M_{B1}}$ are the total deflection at point C, the deflection at point C due to the force F_{r1} alone, the deflection at point C due to the force F_{r2} alone, the deflection at point C due to the moment M_A alone, and the deflection at point C due to the moment M_B alone, respectively. ω_{r2}, $\omega_{P_1 2}$, $\omega_{P_2 2}$, $\omega_{M_{A2}}$, $\omega_{M_{B2}}$ are the total deflection at point D, the deflection at point D due to the force F_{r1} alone, the deflection at point D due to the force F_{r2} alone, the deflection at point D due to the moment M_A alone, and the deflection at point D due to the moment M_B alone, respectively.

Using the beam deflection formula on each force and moment, we have the expressions of ω_{r1}, $\omega_{P_1 1}$, $\omega_{P_2 1}$, $\omega_{M_{A1}}$, $\omega_{M_{B1}}$, ω_{r2}, $\omega_{P_1 2}$, $\omega_{P_2 2}$, $\omega_{M_{A2}}$ and $\omega_{M_{B2}}$. Then, substituting them into (7) and (8), we have

$$\begin{aligned}\omega_{r1} = \frac{1}{6lEI}\big[&-2F_{r1}a_1^2(l-a_1)^2 + F_{r2}a_1b_2\left(a_1^2+b_2^2-l^2\right)\\ &+ M_Aa_1\,(l-a_1)\,(a_1-2l) + M_Ba_1\,(l-a_1)\,(l+a_1)\big]\end{aligned} \tag{9}$$

$$\begin{aligned}\omega_{r2} = \frac{1}{6lEI}\big[&F_{r1}a_1b_2\left(b_2^2+a_1^2-l^2\right) - 2F_{r2}b_2^2(l-b_2)^2\\ &- M_A\,(l-b_2)\,b_2\,(l+b_2) + M_B\,(l-b_2)\,b_2\,(2l-b_2)\big]\end{aligned} \tag{10}$$

During the process of stiffness regulation, the center of force couple is coincident with the joint axis, and $a_1 = b_2 = r$, $F_{r1} = -P$, $F_{r2} = P$. We have

$$\omega_{r2} = -\omega_{r1} = \omega \tag{11}$$

$$T = P(l-2r)\cos\frac{\omega}{2r} \tag{12}$$

where T is the external torque. Then, we have

$$M_A = -\frac{Pr(l-r)(2r-l)}{l^2} \tag{13}$$

$$M_B = M_A \tag{14}$$

$$P = -\frac{6l^3EI\omega}{r^3(l-2r)^2(2l-r)} \tag{15}$$

$$\theta_\delta = \frac{\omega_{r1}-\omega_{r2}}{l-2r} = \frac{2\omega}{l-2r}\quad 0 < r < \frac{1}{2} \tag{16}$$

https://doi.org/10.1017/S0263574717000492 Published online by Cambridge University Press

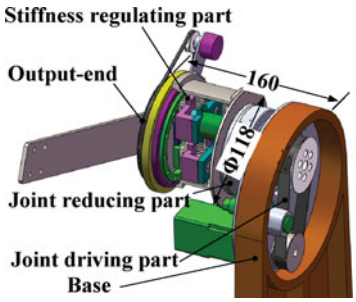

Fig. 3. CAD model of vsaFGR.

where the angular deflection is θ_δ and it is small enough. Substituting (15) into (12), we have

$$T = \frac{6l^3EI\omega}{r^3(l-2r)(2l-r)}\cos\frac{\omega}{2r} \tag{17}$$

The joint stiffness K is defined as

$$K = \frac{dT}{d\theta_\delta} = \frac{3l^3EI\cos\frac{\theta_\delta(l-2r)}{4r}}{r^3\,(2l-r)} \tag{18}$$

The joint stiffness keeps inversely proportional to r^4. Such a high-order function provides the benefit of nonlinearly varying the joint stiffness to obtain a very wide stiffness range but in a short regulating displacement. In our prototype, the regulation displacement r is in the range from 11 mm to 31 mm, the joint stiffness can be regulated from 217 to 3527 N.m/rad.

We have the potential energy P_e stored in the FGR

$$P_e = \frac{K{\theta_\delta}^2}{2} = \frac{T^2}{2K} \tag{19}$$

According to (18), the joint stiffness K is dependent on five factors, such as E, I, r, l and θ_δ . Once the material is specified, E becomes a constant. Once the geometries of FGR are fixed, l and I are also constants. θ_δ is very small that the value of $\cos[\theta_\delta(l-2r)/4r]$ can be considered as 1. So K keeps a (-4) order dependency on the adjusting displacement r. r is linearly proportional to the angular position of the regulating motor σ because of the rack and gear pair, so K is a function of one variable σ, providing ease of regulating the joint stiffness.

4. Prototype Fabrication

Based on the working principle and the mechanics model above, the CAD design has been finished as shown in Fig. 3, where the unit is mm. For a direct overview of the joint actuator, an exploded view of vsaFGR's virtual prototype is shown in Fig. 4, where the mechanical system is explicitly presented.

4.1. Mechanical structure

The mechanical structure of vsaFGR consists of five series-connected parts: the base, the joint driving part, the joint reducing part, the stiffness regulating part and the output-end applied by loads, as shown in Fig. 3. The series-connected patterns provides the convenience of integrating FGR into a robotic joint. The joint driving part installed at the base 4–1 includes a commercial servo motor 4–15 (4–15 means the 15th part in Fig. 4) and a timing belt transmission 4–2. The major component of the joint reducing part is a harmonic gear reducer 4–3, and it is used to set the equilibrium position of the output-end. The stiffness regulating part is serially connected between the joint reducing part and the output-end. It includes the FGR 4–5 and two pairs of stiffness regulating mechanisms 4–4 placed in the symmetric way. The FGR, engaged with the spur gears, is connected at both ends with the hollow

https://doi.org/10.1017/S0263574717000492 Published online by Cambridge University Press

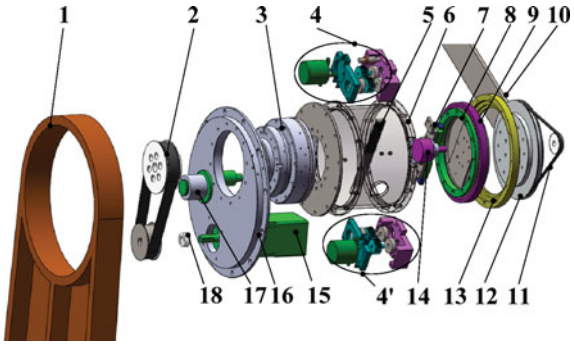

Fig. 4. Exploded view of vsaFGR. 1- Base, 2- Timing belt for driving, 3- Harmonic gear drive, 4- Stiffness regulating mechanism (Details are shown in Fig. 5), 5- Flexible gear rack, 6- Hollow output-shaft, 7- Guide and slider, 8- Inner bushing for bearing, 9- Crossing roller bearing, 10- Output-link, 11- Timing belt for measuring, 12- Output-flange, 13- Outer bushing for bearing, 14- Resistance potentiometer, 15- Joint motor, 16- Mounting flange, 17- Tension wheel, 18- Spacer.

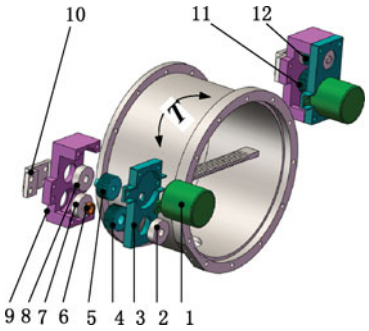

Fig. 5. Stiffness regulating mechanism of vsaFGR. 1- Stiffness regulating motor, 2, 7, 8-Deep groove ball bearing, 3- Cover, 4- Passive gear on the left, 5- Active gear on the left, 6-Bushing, 9-Bracket, 10- Fitting (for slider), 11-Active gear on the right, 12- Passive gear on the right.

output-shaft 4–6. At the equilibrium position, the acting line between the FGR and gears and the axis of the output-end meet at right angles.

The detailed transmission chain of the stiffness regulating part, as shown in Fig. 5, is described as the stiffness regulating motor 5–1 → the spur gear 5–5, 5–11 (engaged with the FGR 4–5) → the slider 5–10 (connected with the bracket 5–9 by fitting) → the guide 4–7→ the output-flange 4–12 (supported by the crossing roller bearing 4–9 and homocentric with the harmonic gear drive 4–3) → the output-link 4–10. When the motors rotate, the gears are translated along the FGR 4–5. Then the distance between the two sliders is varied, and the rotational stiffness of the joint actuator is regulated.

Each stiffness regulating motor drives one pair of spur gears, which are placed in the symmetric way along the FGR and connected by the bracket 5–9, as shown in Fig. 5. On the left pair of spur gears, the upper one 5–5 is active and the lower one 5–4 is passive. On the right pair of spur gears, the upper one 5–12 is passive and the lower one 5–11 is active. Each gear is supported by a shaft and bearings. If the joint torque is in the anticlockwise direction, both of the active gears are exerted by the radial forces. Otherwise, both of the passive gears are exerted by the radial forces. If both of the active gears rotate clockwise, the relative displacement between them is reduced to decrease the joint stiffness. On the other hand, the relative displacement is increased to upgrade the joint stiffness. So the joint stiffness in both directions can be regulated independently.

The major specifications of all the components are concluded in Table I.

4.2. Manufacturing process of FGR

FGR, one of the key elements in vsaFGR, will endure fatigue stress and impact loads. Alloy steel is recommended for the material of FGR. To guarantee the both-end clamped constraint, FGR is preferably integrated with the hollow output-flange without any fixtures, and the teeth profile is processed by wire-electrode cutting technology after machining. Appropriate heat treatment is

https://doi.org/10.1017/S0263574717000492 Published online by Cambridge University Press

Table I. Specification of components..

Item	Parameters
Joint motor	Servo motor, 3000 r/min, 0.32 N.m rating
Timing belt for driving	Speed ratio 1.5
Stiffness-regulating motor	Step motor, 24 V, 0.3 A rating, 7.2 Watt
Gearbox for regulating motor	Speed ratio 30
Modulus of gear tooth	0.5 mm
Teeth number of adjusting gear	32
Length of flexible gear rack	$l = 102$ mm
Full stiffness regulation	1.0 second
Cross section of flexible gear rack	Effective height $h = 1.25$ mm, Width $b = 10$ mm, $I = bh^3/12$
Material of flexible gear rack	Alloy steel, $E = 210$ GPa Yield limit $\sigma_s = 930$ MPa Proportional limit $\sigma_k = 550$ MPa

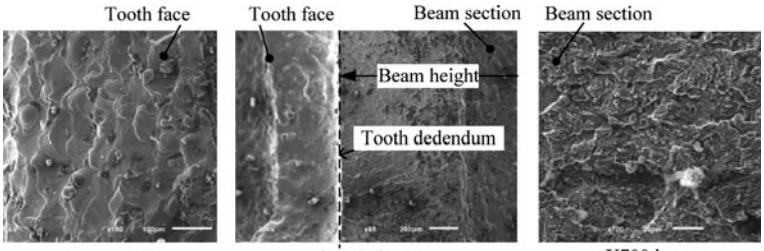

Fig. 6. Electron microscope test of FGR's sectional area.

recommended so that the microstructure in alloy steel is tempered martensite, providing appropriate surface hardness and high elasticity. Applied by the external shock, FGR turns to be the most vulnerable element in the joint actuator. So a copy of FGR is broken off at the critical section by external impact load, and then the electron microscope (JSM-6010) is used for failure analysis. Three magnifications of X65, X180 and X700 are shown in Fig. 6. In Fig. 6(a), the roughness of tooth face is influenced by the wired-electrode technology. In Fig. 6(b), it is found to be cleavage fractures, and brittle fractures are most likely to happen. And there is no micro crack in Fig. 6(c). In conclusion, among all design factors including material choice, cutting process, heat treatment application and geometrical dimension, the most significant factor to prevent brittle fractures is the height of the beam section. If there are severe impacts in the environment, the effective height of FGR has to be increased.

4.3. Specification of vsaFGR

The prototype of vsaFGR has been built, as shown in Fig. 7. With the integration of all elements into the joint actuator, the joint actuator specifications are shown in Table II. Under condition of similar stiffness range, the diameter and the overall volume of vsaFGR is smaller than those of VSJ[37] by 19% and by 27%, respectively. It is worth noting that the power of the regulating motor of VSJ is 200 W, but the regulating power of vsaFGR is only $7.2 \times 2 = 14.4$ W. These small regulating motors not only reduce the dimension of the prototype, but also cut the power demand a lot.

4.4. Sensors of vsaFGR

Different sensors are used to measure the states of vsaFGR. A resistance potentiometer is mounted on the hollow output-shaft, and is connected to the output-flange via a timing belt drive. Its teeth ratio is 5. It is used to detect the actual angular deflection. The sampling resolution of A/D module is 16 bit.

Additionally, the digital interface embedded in the servo amplifier is used to measure the actual speed and the actual position of the joint motor. The incremental encoder of the joint motor is connected to its amplifier, and its resolution is 2500 pulse/revolution. A proximity switch is used for homing. The joint incremental position is scaled with respect to this zero mark.

https://doi.org/10.1017/S0263574717000492 Published online by Cambridge University Press

Table II. Specification of vsaFGR.

Item	vsaFGR	VSJ (37)
Dimension, mm^3	$\Phi 118 \times 160$	$\Phi 146 \times 144$
Weight (except base), Kg	5.1	4.95
Stiffness range, N.m/rad	217–3527	252–3647
Range of joint rotation, $^\circ$	-180 ± 180	-180 ± 180
Peak torque, N.m	9.6	30
Joint motor power, Watt	200	200
Regulating power, Watt	14.4	200
Rotational speed rating, r/min	30	11
Max. deflection, $^\circ$	-2.5 ± 2.5	-11 ± 11
Max. energy Storage, J	0.22	–

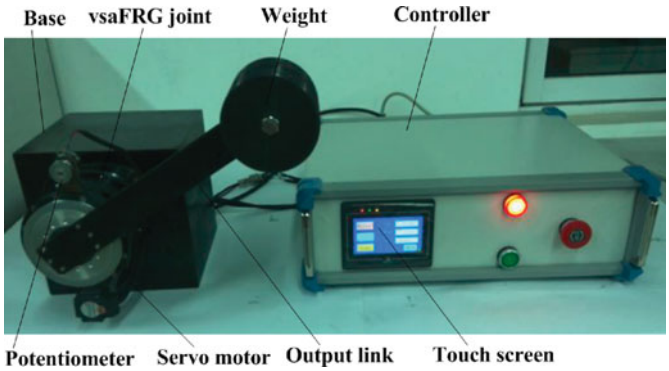

Fig. 7. Prototype of vsaFGR.

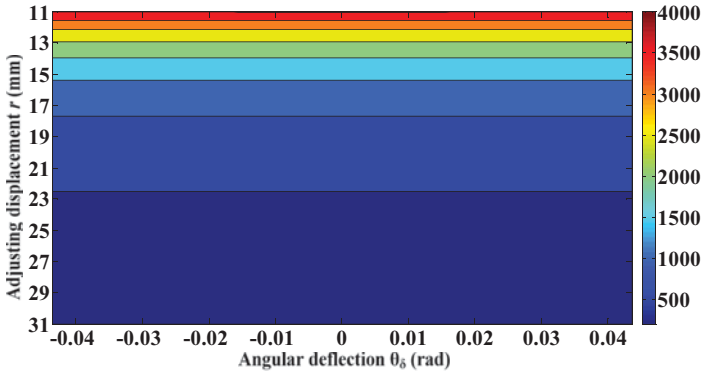

Fig. 8. vsaFGR stiffness as a function of adjusting displacement and angular deflection.

5. Simulation

MATLAB software is used to simulate the joint stiffness in terms of the adjusting displacement, the angular deflection and the moment of inertia of FGR. The potential energy of vsaFGR is also investigated. Then, the joint stiffness is simulated in FEM software.

5.1. Joint stiffness

Based on Eq. (18), the stiffness level of vsaFGR can be regulated by changing the adjusting displacement or the angular deflection. It is shown in Fig. 8 that the general relationship among the adjusting displacement r, the angular deflection θ_δ, and the joint stiffness K. It is found that K primarily depends on r, and the dependency on θ_δ could be negligible. K is a monotonic decreasing function of r. when $r = 31$ mm, the minimum joint stiffness $K_{\min} = 221$ N.m/rad. When $r = 11$ mm, the maximum joint stiffness $K_{\max} = 4034$ N.m/rad. The ratio between the maximum and the minimum stiffness is 20.07 in simulation while the regulating stroke is 20 mm.

https://doi.org/10.1017/S0263574717000492 Published online by Cambridge University Press

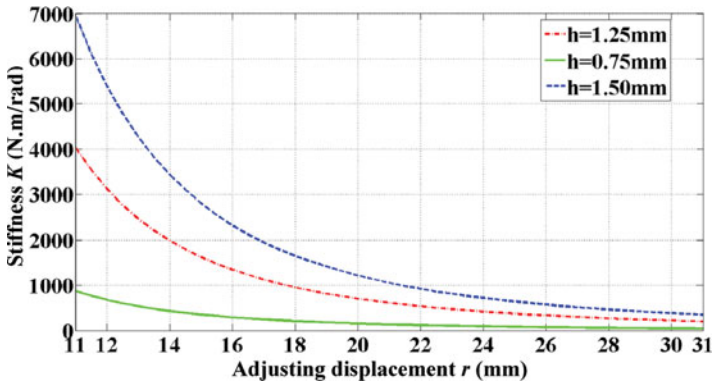

Fig. 9. Joint stiffness relating to effective height of rack.

In Fig. 8, it can be seen that the joint stiffness is nearly independent on the angular deflection θ_δ. K is an even function of θ_δ. For example, if $r = 11$ mm, $K_{11-1} = 4022$ N.m/rad ($\theta_\delta = -2.5^\circ$), $K_{11-2} = 4034$ N.m/rad ($\theta_\delta = 0^\circ$), and $K_{11-3} = 4022$ N.m/rad ($\theta_\delta = 2.5^\circ$). Among them, the relative error is less than 0.3%. If $r = 31$ mm, the relative error is even diminishing. So, the variation of joint stiffness due to the angular deflection can be ignored when the angular deflection is small. vsaFGR can sustain the stable joint stiffness regardless of positive or negative angular deflections corresponding to the varying joint torques.

5.2. Moment of inertia

The moment of inertia I is significantly decided by the height of FGR h. The relationship among the adjusting displacement r, the effective height of FGR h, and the joint stiffness K is illustrated in Fig. 9 when $\theta_\delta = 0$. Appropriate h could be designed to satisfy the application requiring a very big or a very small joint stiffness range. As an alternative, the both-end constraint of FGR could be modified into the one-end fixed type to shift the stiffness range to an expected area. This vsaFGR prototype will be used to simulate an ankle joint, with $h = 1.25$ mm (the dash dot curve in Fig. 9) with both-end clamping.

When $h = 0.75$ mm, $h = 1.25$ mm and $h = 1.5$ mm, the ratios between the maximum stiffness and the minimum stiffness are 20.07. So, although the value of h plays a significant role in deciding the joint stiffness, there are no effects on the stiffness ratio. Poor fatigue strength will be shown in the case of $h = 0.75$ mm. If severe shock exist, $h = 1.5$ mm is recommended.

5.3. Potential energy

By Eq. (19), the potential energy P, stored in FGR, has been explored, as shown in Fig. 10. At the minimum joint stiffness and the maximum torque, the maximum potential energy $P = 0.22$ J. If vsaFGR collides with the environment, it will absorb a reasonable amount of kinetic energy to avoid further damage. The stored potential energy could be used to speed up the output-link, which will be demonstrated in the experiment of Section 6.

The maximum potential energy seems small. The main reason is the angular deflection. First, it must be small enough to satisfy the linear model in Section 3. The second reason is the both-end clamping constraint. The critical section of FGR is at both ends without any slop. The tensile stress must be below the proportional limit of the material to guarantee that FGR is working in its elastic range.

5.4. FEM Simulation of joint stiffness

The stress analysis of FGR is done by the ABAQUS software, shown in Fig. 11(a). The material choice of FGR is alloy steel, ISO 59Si7. The solid element is chosen. The contact between the gear and the rack is simplified as the contact between a cylinder and a plane. FGR is fixed at both ends. When the applied torque is 9.0 N.m, the maximum stress on FGR is 330 MPa, which shows that it is still in its proportional limit. The radial deflection of meshing points is about 0.179 mm based on the strain analysis in Fig. 11(b) when the theoretical joint stiffness is 4034 N.m/rad. The simulated

https://doi.org/10.1017/S0263574717000492 Published online by Cambridge University Press

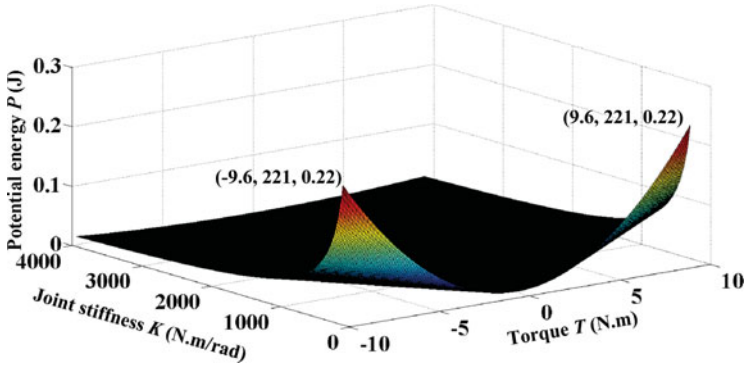

Fig. 10. Potential energy of vsaFGR.

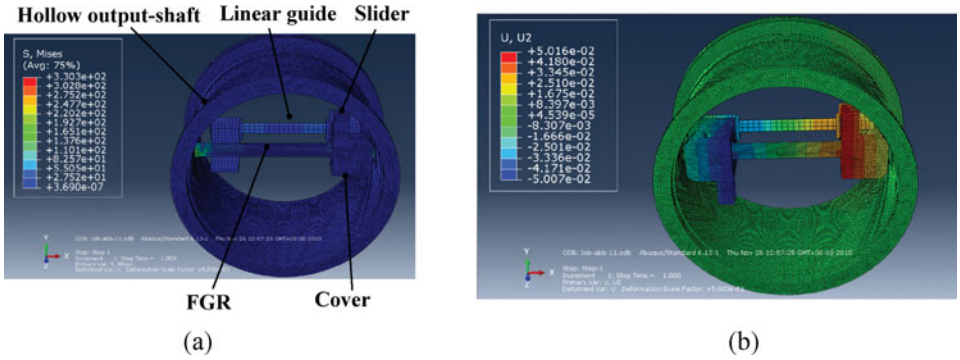

Fig. 11. FEM Simulation of vsaFGR. (a) Stress analysis. (b) Strain analysis.

stiffness is 4001 N.m/rad. A group of virtual torques is applied on vsaFGR, and the corresponding joint deflection is measured, then the joint stiffness is computed. The virtual joint stiffness is shown in Fig. 12(b) in "□" marks. At the lower joint stiffness, the simulation results keep nearly the same as the theoretical curve, but as the stiffness grows, the simulation error increases. Given that the contact stiffness between the linear guide and the slider, and other machine elements are not ideally rigid, they are regarded as flexible elements connected between FGR and the base. The simulation error is mainly caused by them.

6. Experiment

A prototype of vsaFGR and its control system, as shown in Fig. 7, have been developed to investigate its performance through experiments. A mirco controller with 500 MHz frequency has been used for the position control, A/D sampling and interface communication.

The control system is mainly based on a position controller, where the inputs are the desired joint stiffness K_d and the nominal link position θ_n. A set point control with the joint motor's angular position feedback is adopted. The Proportion-Integral-Derivative (PID) control scheme is adopted for accurate position control of the joint motor. The PID gains of the position loop are tuned experimentally to perform high response and stable action. The actual position, speed and torque of the joint motor are fed back via its amplifier interface to the micro controller. The actual angular deflection of the output-link θ_δ is also fed back to the micro controller via the resistance potentiameter. The sum of θ_n and θ_δ is the actual position of the output-link.

The open-loop position control is adopted for the two regulating motors. The desired position of the regulating motor is decided by the desired joint stiffness K_d. It is also calculated on the host computer, and downloaded in the RAM area of the controller. Three experiments of stiffness regulation, position response, and trajectory tracking are conducted.

https://doi.org/10.1017/S0263574717000492 Published online by Cambridge University Press

Table III. Static stiffness fitting of vsaFGR.

	K_r (N.m/rad)			
R (mm)	Actual K_{r-a}	Theoretical K_{r-t}	ϵ	R
11	3527	4034	−0.13	0.999
15	1412	1625	−0.13	0.997
19	758	816	−0.07	0.998
23	418	470	−0.11	0.999
27	274	297	−0.08	0.999
31	217	221	−0.02	0.998

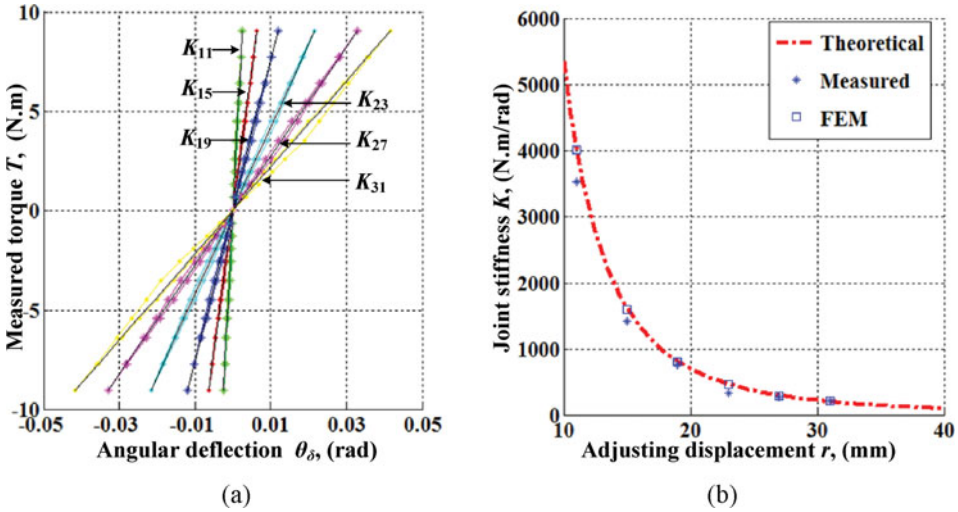

Fig. 12. Stiffness regulation. (a) Torque over angular deflection. (b) Theoretical, measured and simulated stiffness.

6.1. Stiffness regulation

The relationship between the output torque and the angular deflection is measured at the 4-mm interval of the regulating displacement. Brake is applied to the joint motor and the displacements of the regulating motors are controlled. The load torque values are calculated by multiplying the weight of mass and its arm. The angular deflection is detected by the resistance potentiometer. The colored points are the measured data, and linear fitting techniques are used to obtain the actual stiffness profile, as shown in Fig. 12(a). In Table III, the actual stiffness fit by experimental data is compared with the theoretical stiffness obtained by Eq. (18). The relative stiffness error ϵ and the linear correlation coefficient of stiffness fitting process R are also investigated. The linear relationship between the torque and the angular deflection is validated, with the maximum error -13% and the minimum error -2%.

The relative stiffness error ϵ is mainly limited by the structural stiffness of other mechanical components. When the joint stiffness is at a lower stiffness than the structural stiffness of other mechanical components, the measured joint deflection is primarily decided by the regulating mechanism. When the joint stiffness is increased, it is comparable to the structural stiffness of other mechanical components. The measured joint deflection is partly due to other flexible component, which are considered to be rigid in the mechanics model. The linear correlation coefficient R is mainly influenced by the inherent hysteresis of the joint actuator. The backlashes of gear-rack engagements and the material hysteresis contribute a lot to the stiffness hysteresis as shown in Fig. 12(a). The stiffness hysteresis is dependent on the angular deflection. The angular deflection is greater at a lower level of joint stiffness than at a higher level, so the stiffness hysteresis is more significant at a lower level of joint stiffness than at a higher level. The material with litter hysteresis behavior is recommended to manufacture the FGR. Narrow tolerance of gears and FGR are required during manufacturing process, and backlash compensation is also required in the position control of the regulating motors.

https://doi.org/10.1017/S0263574717000492 Published online by Cambridge University Press

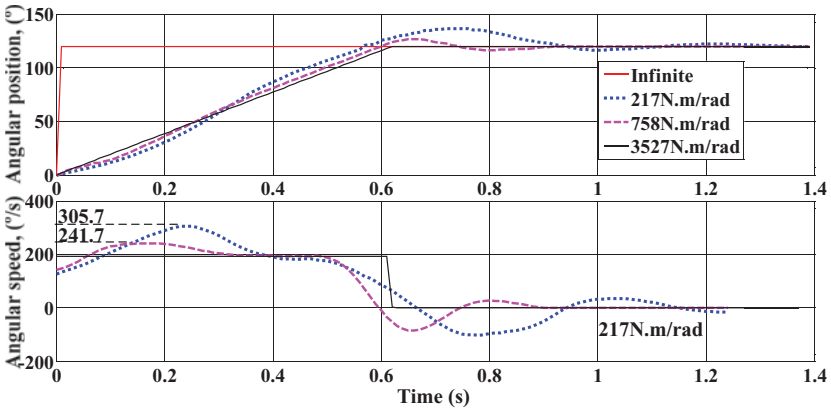

Fig. 13. Step response of position control.

It is found in Fig. 12(b) that the theoretical stiffness is bigger than both the measured one and the simulated one. The potential reason is the stiffness model, as well as the flexibility of other mechanical components, the gear position error and the machining inconsistency of FGR's height. In the stiffness model of Eq. (18), only the deflection of FGR has been considered. In the FEM analysis, most of the mechanical components are meshed and regarded as flexible. FEM model is more closed to the physical prototype. So, the stiffness error between the measured and FEM is smaller than that between the measured and the stiffness model. To increase the accuracy of stiffness regulation, it is desired that the stiffness of other components should be much higher than the flexible component. With the increase of joint stiffness, we've found that the error between the simulation and the experiment is growing. The max error is −13% at the highest level of joint stiffness. The main reason is the backlash in timing belt transmission, the backlash in rack and gear mechanism, and the sampling resolution of the angular deflection.

6.2. Position control

To investigate the performance of position control, the step responses for an amplitude of 120° are investigated with the minimum and maximum joint stiffness. A weight, whose inertia is 0.31 kg.m^2, is attached to the output-link of vsaFGR. The joint motor is controlled to perform the step move and the angular deflection of the output-flange is measured in real time. As shown in the upper half of Fig. 13, the vibration is controlled by the variable joint stiffness. The overshoot at the maximum joint stiffness (1°) is much smaller than that at the minimum joint stiffness (16°). When the stiffness is maximum (3527 N.m/rad), vibration does hardly occur, and the settling time is about 0.6 s. However, when the stiffness is minimum (217 N.m/rad), damped vibration occurs obviously, and the settling time is about 1.3 s. Because of the vibration, the settling time with the minimum stiffness is longer than that of the maximum stiffness. As the joint stiffness is decreased, the damped nature frequency of the vibration is also decreased. Model uncertainty such as backlash of gear engagements, friction force and nonlinearity of timing belt drive cause steady-state errors.

The speed-up behavior of vsaFGR has been controlled by the variation of joint stiffness through further experimental results in the lower part of Fig. 13. If the output-link is rigidly connected to the output-flange, the maximum speed of the output-link is not above the maximum speed of the output speed of the reducer. However, a higher output-link speed is achieved when FGR is placed between the output-flange and the output-shaft because the elastic energy stored in the flexible rack is converted to the kinetic energy of the output-link. As shown in Fig. 13, the peak speed of the link is 305.7°/s with the minimum joint stiffness, and is 54% higher than the output speed of the joint reducer (195°/s). It is 241.7°/s with the joint stiffness of 758 N.m/rad, and it is 24% higher than the output speed of the joint reducer. So, lower stiffness provides more benefits for a walking action.

6.3. Trajectory tracking

Experiments on tracking a typical cosine trajectory with an amplitude of 60° and a period of 1.2 s are conducted under the minimum and the maximum stiffness conditions. A 2.40 kg mass is installed at

https://doi.org/10.1017/S0263574717000492 Published online by Cambridge University Press

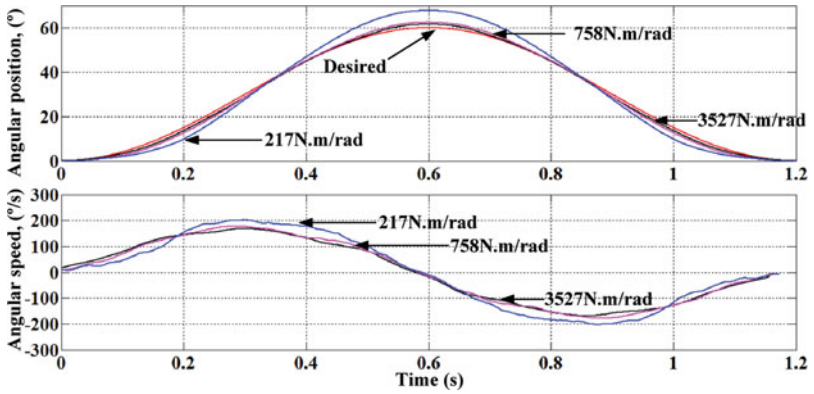

Fig. 14. Trajectory tracking in horizontal plane.

the output-link, and the length of the output-link is 250 mm. The joint motor is controlled to perform the cosine move and measure the angular deflection of the output-flange.

When the VSA is attached to the horizontal frame, there is no effect of gravitational force but the inertia force caused by the moving mass. The inertial force is regarded as the loading force, and a loading torque is applied on the output-end. There is no angular deflection at the start of motion. In Fig. 14, the overshoot error is 8.0° with the minimum stiffness (217 N.m/rad), while with the maximum stiffness (3527 N.m/rad), the overshoot is 1.4°. At the beginning of the move, the actual speed of the output-end is smaller than the desired. That's because that the kinetic energy of the joint motor is converted into the potential energy of FGR. After a while, the converting process of energy is reversed. The potential energy is converted into the kinetic energy. At the time of 0.2 s, the actual speed of the output-end is higher than the desired. The speed-up feature of vsaFGR provides benefits to walking robots, but also bring inconvenience of accurate position control. When the joint stiffness is decreased, the tracking error is increased. How to control the accuracy of trajectory tracking requires more future research work.

Furthermore, the peak speed is also investigated at different joint stiffness. At the minimum stiffness (217 N.m/rad), the peak speed is 202°/s corresponding to the kinetic energy of 0.93 J of the mass, while at the maximum stiffness (3527 N.m/rad), the peak speed is 168°/s corresponding to the kinetic energy of 0.65 J. So the lower the joint stiffness, the more potential energy stored and then converted into kinetic energy. The increment of the kinetic energy between the maximum stiffness and the minimum stiffness is 0.28 J, which is reasonably matched with the simulated results of potential energy. So for a walking robot, it provides feasibilities of varying the joint stiffness appropriately to adapt to the leg's speeding-up action given a specific input power.

7. Conclusion and Future Works

In order to reduce the dimension and the power cost of VSA, a new vsaFGR is proposed based on the flexible gear-and-rack mechanism. The major novelty of vsaFGR lies in that the elastic element and the adjusting mechanism are combined into the FGR, providing the compactness of the mechanical structure. Second, the apparent stiffness of the joint and the output position can be regulated in an uncoupling way by introducing the flexible gear-and-rack mechanism. The joint stiffness is not only nearly independent from the joint position and the joint angular deflection, but also provides the benefits of nonlinearly regulating joint stiffness in a large rang (from 217 to 3527 N.m/rad) but in a short stroke (20 mm). Finally, the gear displacement is perpendicular to the joint loading force, so the power cost required by the stiffness regulation is very low (as low as 14.4 W), providing the promising potential of energy saving. The model of nonlinear factors such as the gear backlash and the flexibility of other components will be studied to improve the accuracy of the joint stiffness. Especially, when the joint stiffness is at the highest level, the angular deflection of the joint could be very small, at the same level of the backlash and the deformation of other mechanical elements. These nonlinear factors could be dominant in regulating the joint stiffness. This is the main disadvantage of our proposed

https://doi.org/10.1017/S0263574717000492 Published online by Cambridge University Press

regulating mechanism. vsaFGR may be used to act as an ankle joint in the future humanoid robot, and the dynamic performance will be investigated in the future work.

Acknowledgments
This work was supported by the Natural Science Foundation of China (No. 51305008).

References

1. G. Grioli, S. Wolf, M. Garabini, M. Catalano, E. Burdet, D. Caldwell, R. Carloni, W. Friedl, M. Grebenstein, M. Laffranchi, D. Lefeber, S. Stramigioli, N. Tsagarakis, M. van Damme, B. Vanderborght, A. Albu-Schaeffer and A. Bicchi, "Variable stiffness actuators: The user's point of view," *Int. J. Robot. Res.* **34**(6), 727–743 (2015).
2. D. Lefeber, "Use of Compliant Actuators in Robotic Applications," Proceedings of IEEE Conference on Advanced Technologies for Enhanced Quality of Life, Iasi, Romania (2009) pp. 22–22.
3. B. Vanderborght, A. Albu-Schaeffer, A. Bicchi, E. Burdet, D. G. Caldwell, R. Carloni, M. Catalano, O. Eiberger, W. Friedl, G. Ganesh, M. Garabini, M. Grebenstein, G. Grioli, S. Haddadin, H. Hoppner, A. Jafari, M. Laffranchi, D. Lefeber, F. Petit, S. Stramigioli, N. Tsagarakis, M. Van Damme, R. Van Ham, L. C. Visser and S. Wolf, "Variable impedance actuators: A review," *Robot. Auton. Syst.* **61**(12), 1601–1614 (2013).
4. R. V. Ham, S. Thomas, B. Vanderborght, K. W. Hollander and D. Lefeber, "Compliant actuator designs: Review of actuators with passive adjustable compliance/controllable stiffness for robotic applications," *IEEE Robot. Autom. Mag.* **16**(1), 81–94 (Sep. 2009).
5. A. Albu-Schaffer, O. Eiberger, M. Grebenstein, S. Haddadin, C. Ott, T. Wimbock, S. Wolf and G. Hirzinger, "Soft robotics," *IEEE Robot. Autom. Mag.* **15**(3), 20–30 (Sep. 2008).
6. S. Lee, "Development of a new variable remote center compliance (VRCC) with modified elastomer shear pad (ESP) for robot assembly," *IEEE Trans. Autom. Sci. Eng* 2(2), 193–197 (2005).
7. G. A. Pratt and M. M. Williamson, "Series Elastic Actuators," Proceedings of IEEE/RSJ International Conference on Intelligent Robots and Systems 'Human Robot Interaction and Cooperative Robots', Pittsburgh, PA, USA (1995) pp. 399–406.
8. N. G. Tsagarakis, M. Laffranchi and B. Vanderborght, "A Compact Soft Actuator Unit for Small Scale Human Friendly Robots," Proceedings of IEEE International Conference on Robotics and Automation, Kobe, Japan (2009) pp. 4356–4362.
9. M. Laffranchi, N. Tsagarakis and D. G. Caldwell, "A Compact Compliant Actuator (CompAct™) with Variable Physical Damping," Proceedings of IEEE International Conference on Robotics and Automation, Shanghai, China (2011) pp. 4644–4650.
10. A. S. Shafer and M. R. Kermani, "On the feasibility and suitability of MR fluid clutches in human-friendly manipulators," *IEEE/ASME Trans. Mechatronics* **16**(6), 1073–1082 (Dec. 2011).
11. S. Kajikawa and K. Abe, "Robot finger module with multidirectional adjustable joint stiffness," *IEEE/ASME Trans. Mechatronics* **17**(1), 128–135 (Feb. 2012).
12. Y. Du, Z. Fang, Z. Wu and Q. Tian, "Thermomechanical Compliant Actuator Design using Meshless Topology Optimization," *Proceedings of Asia Simulation Conference-7th International Conference on System Simulation and Scientific Computing*, Beijing, China (2008) pp. 1018–1025.
13. J. Choi, S. Park, W. Lee and S.C. Kang, "Design of a Robot Joint with Variable Stiffness," *Proceedings of IEEE International Conference on Robotics and Automation*, Pasadena, CA, USA (2008) pp. 1760–1765.
14. S. Kianzad, M. Pandit, J. Lewis, A. Berlingeri, K. Haebler and J. Madden, "Variable Stiffness Structure using Nylon Actuators Arranged in a Pennate Muscle Configuration," Proceedings of the International Society for Optics and Photonics on SPIE Smart Structures and Materials+ Nondestructive Evaluation and Health Monitoring, San Diego, California, United States (2015) pp. 94301Z–94301Z-5.
15. K. Koganezawa, T. Inaba and T. Nakazawa, "Stiffness and Angle Control of Antagonistially Driven Joint," Proceedings of The First IEEE/RAS-EMBS International Conference on Biomedical Robotics and Biomechatronics, Pisa, Italy (2006) pp. 1007–1013.
16. G. Tonietti, R. Schiavi and A. Bicchi, "Design and Control of a Variable Stiffness Actuator for Safe and Fast Physical Human/robot Interaction," Proceedings of the 2005 IEEE International Conference on Robotics and Automation, Barcelona, Spain (2005) pp. 526–531.
17. R. Schiavi, G. Grioli, S. Sen and A. Bicchi, "VSA-II: A Novel Prototype of Variable Stiffness Actuator for Safe and Performing Robots Interacting with Humans," Proceedings of IEEE International Conference on Robotics and Automation, Pasadena, CA, USA (2008) pp. 271–276.
18. J. Hurst and A. Rizzi, "Series compliance for an efficient running gait," *IEEE Robot. Autom. Mag.* **15**(13), 42–51 (Sep. 2008).
19. C. Chou and B. Hannaford, "Measurement and modeling of mckibben pneumatic artificial muscles," *IEEE Trans. Robot. Autom.* **12**(1), 90–102 (Feb. 1996).
20. O. Eiberger, S. Haddadin, M. Weis, A. Albu-Schäffer and G. Hirzinger, "On Joint Design with Intrinsic Variable Compliance: Derivation of the DLR QA-Joint," Proceedings of IEEE International Conference on Robotics and Automation, Anchorage, AK, USA (2010) pp. 1687–1694.

21. X. Zhou, J. Seung-kook, and K. Venkat, "A cable based active variable stiffness module with decoupled tension," *J. Mech. Robot.* **7**(1), 011005–011009 (Feb. 2015).
22. A. Jafari, N. G. Tsagarakis, B. Vanderborght and D. G. Caldwell, "A Novel Actuator with Adjustable Stiffness (AwAS)," *Proceedings of IEEE/RSJ International Conference on Intelligent Robots and Systems*, Taipei, Taiwan (2010) pp. 4201–6206.
23. B. S. Kim and J. B. Song, "Hybrid Dual Actuator Unit: A Design of a Variable Stiffness Actuator based on an Adjustable Moment Arm Mechanism," Proceedings of IEEE International Conference on Robotics and Automation, Anchorage, AK, USA (2010) pp. 34–40.
24. B. S. Kim and J. B. Song, "Design and control of a variable stiffness actuator based on adjustable moment arm," *IEEE Trans. Robotics* **28**(5), 1145–1151 (Oct. 2012).
25. L. Visser, R. Carloni, R. Unal and S. Stramigioli, "Modeling and Design of Energy Efficient Variable Stiffness Actuators," *Proceedings of IEEE International Conference on Robotics and Automation*, Anchorage, AK, USA (2010) pp. 4321–4327.
26. Amir Jafari, N. G. Tsagarakis, I. Sardellitti and D. G. Caldwell, "A new actuator with adjustable stiffness based on a variable ratio lever mechanism," *IEEE/ASME Trans. Mechatronics* **19**(1), 55–63 (Feb. 2014).
27. S. S. Groothuis, G. Rusticelli, A. Zucchelli, S. Stramigioli and R. Carloni. "The variable stiffness actuator vsaUT-II: Mechanical design, modeling, and identification," *IEEE/ASME Trans. Mechatronics* **19**(2), 598–597 (Apr. 2014).
28. N. Vuong, R. Li, C. Chew, A. Jafari and J. Polden. "A novel variable stiffness mechanism with linear spring characteristic for machining operations," *Robotica* **35**(7), 1627–1637 (Jul. 2017).
29. K. Hollander, T. Sugar and D. Herring, "Adjustable Robotic Tendon using a Jack Spring," Proceedings of the 9th IEEE International Conference on Rehabilitation Robotics, Chicago, IL, USA (2005) pp. 113–118.
30. R. V. Ham, M. V. Damme, B. Verrelst and D. Lefeber, "MACCEPA, the mechanically adjustable compliance and controllable equilibrium position actuator: Design and implementation in biped robot," *Robot. Auton. Syst.* **55**(10), pp. 761–768 (Mar. 2007).
31. S. Wolf and G. Hirzinger, "A New Variable Stiffness Design: Matching Requirements of the Next Robot Generation," *Proceedings of IEEE International Conference on Robotics and Automation*, Pasadena, CA, USA (2008) pp. 1741–1746.
32. J. Park and J. Song, "Safe Joint Mechanism using Inclined Link with Springs for Collision Safety and Positioning Accuracy of a Robot Arm," *Proceedings of IEEE International Conference on Robotics and Automation*, Anchorage, AK, USA (2010) pp. 813–818.
33. F. Petit, W. Friedl, H. Hoppner and M. Grebenstein, "Analysis and synthesis of the bidirectional antagonistic variable stiffness mechanism," *IEEE/ASME Trans. Mechatronics* **20**(2), 684–695 (Apr. 2015).
34. A. Alazmani, D. Keeling and P. Walker, "Design and evaluation of a buckled strip compliant Actuator," *IEEE/ASME Trans. Mechatronics* **18**(6), 1–8 (Dec. 2013).
35. T. Morita and S. Sugano, "Development of 4-D.O.F. Manipulator using Mechanical Impedance Adjuster," *Proceedings of IEEE International Conference on Robotics and Automation*, Minneapolis, Minnesota, USA (1996) pp. 2902–2907.
36. M. Yalcin, B. Uzunoglu, E. Altintepe and V. Patoglu, "VNSA: Variable Negative Stiffness Actuation based on Nonlinear Deflection Characteristics of Buckling Beams," *Proceedings of IEEE/RSJ International Conference on Intelligent Robots and Systems*, Tokyo, Japan (2013) pp. 5418–5424.
37. J. Choi, S. Hong, W. Lee and S. Kang, "A robot joint with variable stiffness using leaf springs," *IEEE Trans. Robotics* **27**(2), 229–238 (Apr. 2011).
38. S. Groothuis, R. Carloni and S. Stramigioli, "A novel variable stiffness mechanism capable of an infinite stiffness range and unlimited decoupled output motion," *Actuators* **3**(2), 107–123 (Jun. 2014).
39. W. Wang, X. Fu, Y. Li, and C. Yun, "Design of variable stiffness actuator based on modified Gear–Rack mechanism," *J. Mechanisms Robot., ASME Trans.* **8**(6), 061008-1-10 (Dec. 2016).